Eur. Phys. J. B **18**, 343–352 (2000)

THE EUROPEAN PHYSICAL JOURNAL B

EDP Sciences

Velocity measurement of a settling sphere

N. Mordant and J.-F. Pinton[a]

École Normale Supérieure de Lyon, Laboratoire de Physique[b], 46 Allée d'Italie, 69007 Lyon, France

Received 12 April 2000 and Received in final form 13 July 2000

Abstract. We study experimentally the motion of a solid sphere settling under gravity in a fluid at rest. The particle velocity is measured with a new acoustic method. Variations of the sphere size and density allow measurements at Reynolds numbers, based on limit velocity, between 40 and 7 000. At all Reynolds numbers, our observations are consistent with the presence of a memory-dependent force acting on the particle. At short times it has a $t^{-1/2}$ behaviour as predicted by the unsteady Stokes equations and as observed in numerical simulations. At long times, the decay of the memory (Basset) force is better fitted by an exponential behaviour. Comparison of the dynamics of spheres of different densities for the same Reynolds number show that the density is an important control parameter. Light spheres show transitory oscillations at $Re \sim 400$, but reach a constant limit speed.

PACS. 06.30.Gv Velocity, acceleration, and rotation – 43.60.+d Acoustic signal processing – 47.27.Vf Wakes

1 Introduction

The problem of evaluating the hydrodynamic forces on a rigid body in a moving fluid is a long standing issue. It arises in several engineering domains which involve multiphase flows, *e.g.*, in sedimentation, or improvement of combustion or in the minimization of erosion by droplets in large turbines. All these problems are concerned with the dispersion of particles, whose modeling requires some understanding of the particle dynamics. Another question is the ability of dispersed solid particles to follow the fluid motion when their density or initial velocity do not quite match the fluid properties, that is the ability of solid particles to behave as Lagrangian tracers of fluid motion. This issue is of importance for the prediction of dispersion of pollutants in the atmosphere or in measurement techniques such as particle image velocimetry (PIV). Our own motivation comes from work aiming at developing a Lagrangian tracking technique for the motion of a few solid particles during large intervals of times, in a turbulent flow. It raises the question of the response of a particle to rapid changes in the velocity of the fluid, or to a sudden acceleration.

Analytical approaches to the time-dependent motion of a solid particle in a given fluid flow have been restricted to zero or small Reynolds numbers. However, they provide a general frame of description of the forces acting on the particle. We briefly recall their main results, as a basis for the analysis of our experiments. Consider the motion of a solid body in a general time-dependent flow: external and hydrodynamic forces set the body into motion, and this motion in turn modifies the fluid flow since it introduces a moving boundary condition. The equation of motion for the viscous fluid are the Navier-Stokes equations supplemented by boundary conditions at infinity (in free space) and on the solid body. In order to solve this problem, the general approach is to obtain expressions for the forces on the particle, in terms of the properties of the fluid flow in its absence. Perturbative developments are made, in which the stress tensor is split into contributions from the undisturbed flow and corrections due to fluid motion induced by the particle displacement. The complexity of the problem stems from the calculation of the latter term which contains the history of the particle motion.

In the limit of vanishing Reynolds numbers, Maxey and Riley [1] have proposed for the equation of motion of the particle :

$$m_{\rm p}\frac{{\rm d}\mathbf{v}_{\rm p}}{{\rm d}t} = (m_{\rm p}-m_{\rm f})\mathbf{g} + m_{\rm f}\frac{{\rm D}\mathbf{u}}{{\rm D}t} + 6\pi a\mu_{\rm f}(\mathbf{u}-\mathbf{v}_{\rm p}) + \frac{1}{2}m_{\rm f}\frac{{\rm d}(\mathbf{u}-\mathbf{v}_{\rm p})}{{\rm d}t} + 6a^2(\pi\mu_{\rm f}\rho_{\rm f})^{\frac{1}{2}}\int_0^t \frac{\frac{{\rm d}(\mathbf{u}-\mathbf{v}_{\rm p})}{{\rm d}\tau}}{(t-\tau)^{\frac{1}{2}}}{\rm d}\tau, \quad (1)$$

where $\rho_{\rm f}$ is the density of the fluid, $\mu_{\rm f}$ its viscosity, $\mathbf{u}$ the undisturbed flow field, $\mathbf{v}_{\rm p}$ is the sphere velocity ($\mathbf{u}-\mathbf{v}_{\rm p}$ is the slip velocity), a its radius, $m_{\rm p}$ its mass and $m_{\rm f}$ is the mass of the fluid displaced by the sphere ($m_{\rm f} = (4/3)\pi a^3\rho_{\rm f}$). As customary, we note ${\rm d}\mathbf{v}_{\rm p}/{\rm d}t$ the acceleration of the particle and ${\rm D}\mathbf{u}/{\rm D}t \equiv (\partial_t + \mathbf{u}.\nabla)\mathbf{u}$ that of the fluid. This expression is established for non-uniform non stationary creeping flow, and providing that $\rho_{\rm f}aW_0/\mu_{\rm f} \ll 1$, $\rho_{\rm f}a^2U/(\mu_{\rm f}L) \ll 1$ and $a/L \ll 1$ (U is an

[a] e-mail: pinton@ens-lyon.fr
[b] CNRS UMR 5672

order of magnitude of the velocity of the fluid, W_0 is an order of magnitude of $\mathbf{u}-\mathbf{v}_\mathrm{p}$ and L is a representative differential length scale of the unperturbed flow). Note that when $\mathbf{u}=0$, equation (1) reduces to the historical Basset (1888), Boussinesq (1903) and Oseen (1927) expression for the rectilinear fall of a sphere in a fluid at rest, again in the limit $Re \to 0$ – here, $Re = 2aU/\nu$ with U the limit velocity. The above expression neglects the effects of rotation of the particle. We will do the same throughout this work as we do not observe lift effects in our measurements.

Equation (1) has a "canonical form" in the sense that the terms on the right hand side can be interpreted in a simple way. They are, respectively, gravity, effect of the undisturbed flow, steady drag, added mass and Basset memory integral:

Simple hydrodynamic contribution. The second term corresponds to the forces that would be applied on a fluid particle that would be at the place of the sphere in the undisturbed flow. In the case of a particle settling in a fluid at rest, this term vanishes.

Drag. The steady drag is responsible for the limit velocity of a sphere falling under gravity. The expression in equation (1) is valid only for $Re = 0$. It is well known that for finite Reynolds numbers, the convective inertia increases the drag. The analytic expression is not known for all Reynolds numbers but the empiric law for the drag coefficient as a function of Re is well documented from $Re \to 0$ up to values higher than 10^7. One usually writes the steady drag as :

$$\mathbf{F}_\mathrm{drag} = \frac{1}{2}\pi a^2 \left\|\mathbf{u}-\mathbf{v}_\mathrm{p}\right\| (\mathbf{u}-\mathbf{v}_\mathrm{p}) c_\mathrm{D}(Re), \qquad (2)$$

where c_D is the empiric drag coefficient and Re is the instantaneous Reynolds number based on the slip velocity.

Added mass. The added mass term, classically found in mechanics, is an inertial term and is due to the resistance of the surrounding fluid to acceleration. It has been discussed also by Auton *et al.* [2], Rivero *et al.* [3] and Chang and Maxey [4] who showed that it has to be replaced by

$$\mathbf{F}_\text{added mass} = \frac{1}{2} m_\mathrm{f} \left(\frac{\mathrm{D}\mathbf{u}}{\mathrm{D}t} - \frac{\mathrm{d}\mathbf{v}_\mathrm{p}}{\mathrm{d}t} \right). \qquad (3)$$

The difference is subtle: in equation (1), $\mathrm{d}u/\mathrm{d}t$ refers to the total time derivative of the velocity field following the motion of the sphere, whereas Auton *et al.* [2] use the Lagrangian acceleration of the fluid at the particle location. While the issue is still debated, the expression proposed by Auton *et al.* [2], Rivero *et al.* [3] and Chang and Maxey [4] gives all its meaning to the name "added" mass; indeed, in equation (1), the term involves an effective inertial masses: $m_\mathrm{p} + \frac{1}{2}m_\mathrm{f}$ for the sphere and $\frac{3}{2}m_\mathrm{f}$ for the fluid particle. Note that it yields an inertial mass $(m_\mathrm{p} + \frac{1}{2}m_\mathrm{f})$ that is different from the gravitational mass $(m_\mathrm{p} - m_\mathrm{f})$; and very much so in the case of particle with a density close to that of the fluid. We will show in Section 3.5 that such effects may be of importance.

History. Together with the added mass term, the last term traces back to the modification of the base flow due to the motion of the particle. Thus, it *a priori* involves the entire history of the particle motion. In Maxey and Riley's expression, Stokes flows are considered, so that the only transfer mechanism is diffusion. If the Reynolds number is finite, one has to deal with convective inertia even for small values of Re. As noted in Lovalenty and Brady [5], one must then take into account the generation of vorticity on the sphere, its diffusion away from the sphere and finally its advection in the wake. In such cases, it is doubtful that the memory term may be expressed in the form of a convolution with a simple kernel. Lovalenti and Brady's expression involves the relative position of the particle at different times, for all past times. More generally, a kernel may depend of $t-\tau$ but also on $Re(\tau)$ and possibly of other parameters, such as the the density or even the details of the particle trajectory itself.

At small Reynolds numbers analytical developments have converged to the following structure for the equation of motion of the particle:

$$\begin{aligned}(m_\mathrm{p} + \frac{1}{2}m_\mathrm{f})\frac{\mathrm{d}\mathbf{v}_\mathrm{p}}{\mathrm{d}t} &= (m_\mathrm{p} - m_\mathrm{f})\mathbf{g} + \frac{3}{2}m_\mathrm{f}\frac{\mathrm{D}\mathbf{u}}{\mathrm{D}t} \\ &+ \frac{1}{2}\pi a^2 \rho_\mathrm{f} \left\|\mathbf{u}-\mathbf{v}_\mathrm{p}\right\| (\mathbf{u}-\mathbf{v}_\mathrm{p}) c_\mathrm{D}(Re) + \mathbf{F}_\mathrm{history}. \qquad (4)\end{aligned}$$

We will show that this expression remains very useful to interpret observations at much higher Reynolds numbers.

Experimental studies of this problem are scarce. As explained above, the steady drag term comes entirely from experimental measurements of the drag coefficient in the case of a steady flow past a fixed sphere [6]. The added mass term expression has been validated by numerical simulations of Chang and Maxey [4] for a fixed sphere in an accelerated flow. Shridhar and Katz [7] used it to show that measurements of bubble motion yield consistent results for the drag, compared to the classical estimation of the force acting on a fixed object. The question of the history term is more complex. Several numerical studies of Lawrence and Mei [8], Chang and Maxey [4] and Kim *et al.* [9] agree with the existence of a kernel varying as $t^{-\frac{1}{2}}$ for short times. The long time behaviour is more uncertain, probably due to resolution problems. Indeed, as found by Lawrence and Mei [8], the transient between the two regimes is exponential, with a kernel that drops several orders of magnitude before the long time asymptotics is reached. Experimentally these questions have not been addressed although it is well known that particles do reach a limit velocity in a finite time, a fact that cannot be accounted for with a $t^{-\frac{1}{2}}$ kernel.

Our experimental study covers the range of intermediate ($Re \sim 40$) to high Reynolds numbers ($Re \sim 8\,000$), for the problem of the settling sphere. At the onset of motion, we observe the presence of a diffusive Basset force. The particle then leaves this regime and reaches a finite velocity in a characteristic time of the order of $\sqrt{a/g}$. The observed limit velocity is consistent with previous measurements of the drag on a *fixed* sphere. We also show that density effects are important at Reynolds numbers of about 400, *i.e.* near the onset of vortex shedding:

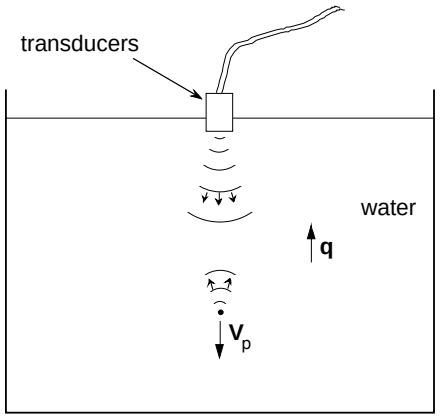

Fig. 1. Experimental setup and principle of measurement.

the velocity of the falling sphere oscillates as it reaches its (steady) limit value.

We present the apparatus and experimental technique, before describing our results in details.

2 Description of the experiment

2.1 Principle

The aim of our experiments is to measure the velocity of a solid sphere falling vertically under gravity in water initially at rest – see Figure 1. The bead is released without any initial velocity or rotation.

The velocity of the particle is detected using a new acoustic method. It is based on the measurement of the Doppler shift of an ultrasonic wave scattered by the moving particle. If one records the scattered ultrasound in a chosen direction, one observes a Doppler shift in the pulsation of the wave

$$\Delta\omega = \mathbf{q} \cdot \mathbf{v}_\mathrm{p}, \tag{5}$$

where $\mathbf{q}$ is the scattering wavevector (the difference between the incident and scattered wavevectors $\mathbf{q} = \mathbf{k}_\mathrm{scat} - \mathbf{k}_\mathrm{inc}$). In the backscattered geometry adopted here, $\mathbf{q} = -2\mathbf{k}_\mathrm{inc}$, so that the frequency shift becomes

$$\Delta\omega(t) = -2\frac{v(t)}{c}\omega_0, \tag{6}$$

where c is the speed of sound, ω_0 is the incident pulsation, and $v(t)$ is the component of the velocity on the incident direction at time t. This is a valid approximation providing that the travel time of the sound between the transducer and the bead is much smaller than the characteristic time of the evolution of the bead's velocity. In our experiment, the largest travel time is of the order of 0.5 ms.

2.2 Experimental set-up

The experiment is performed in a tank of size 1.1 m × 0.75 m and depth 0.65 m, filled with water at rest, see Figure 1. Beads made of glass, steel and tungsten are used. Their specifications and main characteristics of motion are reported in Table 1.

Table 1. Characteristics of the solid spheres and of the experiments. The third column indicates the sphere material: g glass, s steel and w for tungsten carbide. V_l is the limit velocity and σ_{V_l} the corresponding variance. ρ_p is the density of the bead.

#	$2a$		ρ_p	V_l	σ_{V_l}	$\frac{\sigma_{V_\mathrm{l}}}{V_\mathrm{l}}$	Re	τ_{95}
	mm		$\mathrm{kg\,m^{-3}}$	$\mathrm{m\,s^{-1}}$	$\mathrm{mm\,s^{-1}}$	%		ms
1	0.5	g	2560	0.0741	0.4	0.6	41	55
2	1.5	g	2560	0.218	0.9	0.4	360	142
3	2	g	2480	0.271	1	0.5	600	197
4	0.8	s	7710	0.316	3	0.9	280	108
5	1	s	7850	0.383	2	0.5	430	132
6	2	s	7670	0.636	1	0.2	1400	197
7	3	s	7800	0.813	4	0.5	2700	225
8	4	s	7700	0.973	4	0.4	4300	292
9	6	s	7750	1.158	5	0.4	7700	315
10	1	w	14800	0.590	2	0.3	660	148

The bead is held by a pair of tweezers, five centimeters below the transducers. It is released a time $t = 0$ without initial velocity and its trajectory is about 50 cm long. We start the data acquisition before the bead is released in order to capture the onset of motion.

The non-perturbed flow is simply the hydrostatic state. This induces an axisymmetry in the initial condition about the vertical axis that contains the center of the bead. For low Reynolds numbers (say less than 200), the flow around the sphere remains axisymmetric so that the rotation of the bead remains zero. We have observed that the trajectory is vertical and we assume throughout this work that it is rotation free. The Reynolds number based on the sphere diameter and velocity has typical values from 40 to 7700 which are relatively high values for that problem. The limit velocity of the sphere varies from 0.07 to 1.16 $\mathrm{m\,s^{-1}}$.

We use two coplanar arrays of Vermon ultrasonic transducers of size 2×2 mm each, separated by 100 μm. Their resonant frequency is about 3.2 MHz and their bandwidth at −3 dB is 1.5 MHz. This array is placed parallel to the bottom of the tank and 1 cm below the free surface of the water. The emission is toward the bottom of the tank. A function generator Hewlett Packard VXI HP E1445A produces the emission sinusoid at 3.5 MHz or 2.5 MHz (depending on bead size). This signal is sent to one of the ultrasonic transducers. The acoustic wave is backscattered by the falling bead and detected by the second transducer. The received signal is digitized at a sampling rate of 10 MHz and over a 18 bit dynamic range, numerically heterodyned at the emitting frequency and decimated to the chosen sampling frequency by a VXI embedded HP E1430A sampling device driven by a PC.

2.3 Signal processing

For velocities of the order of 0.5 $\mathrm{m\,s^{-1}}$, one expects a Doppler shift of about 2 kHz. As a result of the heterodyning, the frequencies are shifted around zero

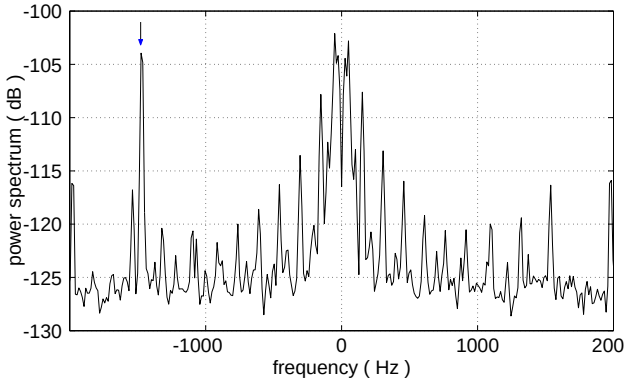

Fig. 2. Power spectrum of the backscattered sound, in the case of steel bead of diameter 0.8 mm, for an incoming sound frequency at 3.5 MHz. In this measurement, the bead has reached its limit velocity. The arrow indicates the particle Doppler shift; spurious frequency lines at harmonics of 50 Hz are also present.

the frequency and the signal is complex. It also contains contributions of reflexions of the incident wave on the walls and at the free surface. The walls do not move and thus do not induce a frequency shift. It was not possible to totally avoid surface waves on the interface air/water but their speed is very low compared with that of the falling bead. Thus the Doppler shift induced by these reflexions is about 15 Hz, small compared to the typical 1 kHz shift due to bead motion. The frequency domains are well separated and it is possible to get rid of reflexions by a numerical lowpass fifth order Butterworth filter of width 25 Hz (the velocity associated to this Doppler shift is 0.005 $\mathrm{m\,s^{-1}}$ for an emitting frequency equal to 3.5 MHz).

Figure 2 shows an example of the power spectrum of the backscattered signal. One can see an intense peak around the incoming frequency (shifted to zero) and a peak in the negative frequency domain corresponding to the sound scattered off the falling bead. The Doppler shift of this latter peak gives the particle velocity.

In order to obtain its time evolution, one must perform a time-frequency analysis. One way is to compute the spectra through a running window, *i.e.* the spectrogram of the signal. An example is given in Figure 3a. This technique captures the evolution of the bead velocity, but the resolution is low, as apparent on the inset of the figure which shows a normalized cross-section of the spectrogram. One way to improve it drastically is to use a method of reassignment of the spectrogram, as described by Auger and Flandrin [10]. In this way one obtains the picture shown in Figure 3b. From it, we extract the function $\Delta\omega(t)$ by simply taking the maximum of amplitude at every time t, and obtain the function $v_{\mathrm{p}}(t)$, shown in Figure 4. Comparison of the inset in Figure 3b with the one in Figure 3a shows that we obtain in this way a 10-fold gain in the precision of the velocity measurement.

In order to estimate the sensitivity of the method, we applied it to synthetic signals modeling the particle dynamics (see next section) to which we added a noise that mimics the experimental data (a white gaussian noise with

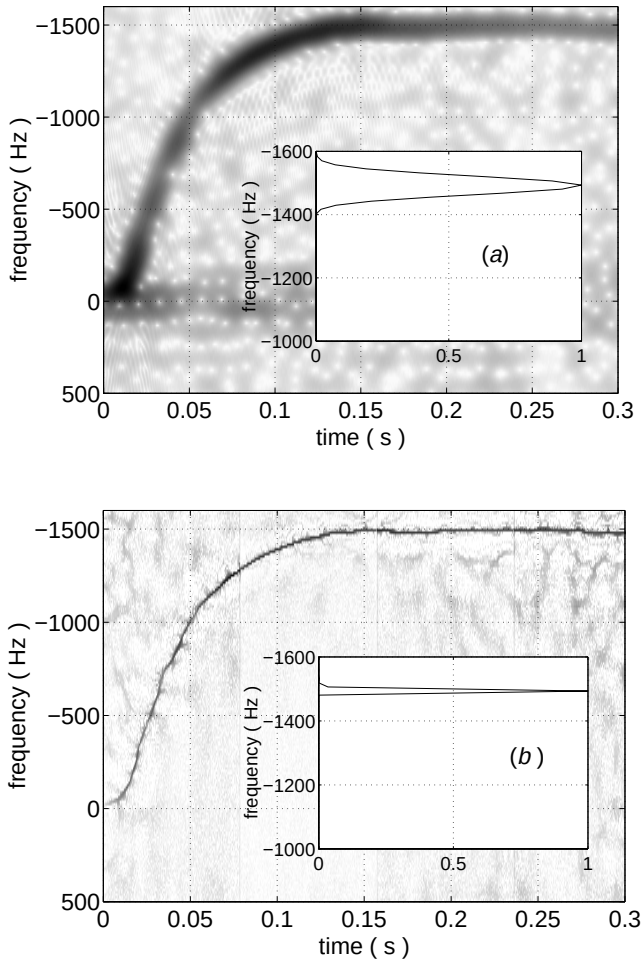

Fig. 3. (a) Spectrogram of the backscattered sound, after heterodyne detection, for the same bead as in Figure 2. (b) Reassigned spectrogram. In each figure the inset shows a normalized cross-section of the spectrogram.

a $1/f$ low frequency noise cut at 25 Hz as in the experiment). The signal to noise ratio for the synthetic signal is equal to that of the experimental data. We observe that the resolution of the measurement (in *rms* units) is of the order of one-half pixel in the time frequency image; it corresponds to a precision of 0.3% on the particle velocity with a time resolution of about 1 ms. Note that the precision is quite reduced at the instant of onset of motion ($t < 5$ ms and $V < 0.02$ m/s), because of the integrating nature of the algorithm.

We can also estimate the measurement error experimentally in the steady regime, when the particle has reached its terminal velocity. It can be estimated in two ways: first, as the fluctuation in the detected Doppler shift during a single fall and, second, as the *rms* variation of the limit velocity measured from a set of 10 falls. This procedure yields a mean *rms* error of 0.5% on the particle velocity, as indicated in Table 1.

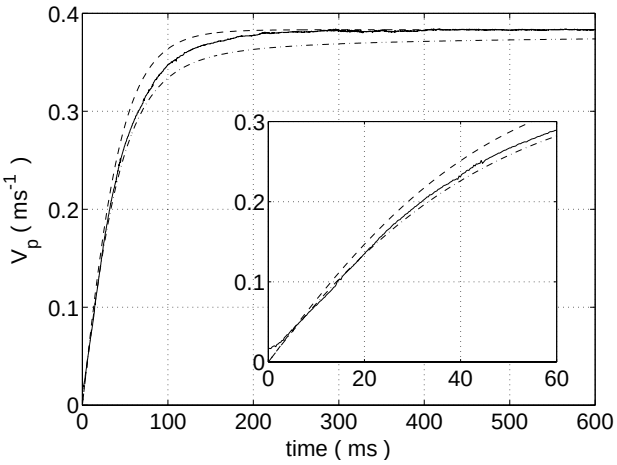

Fig. 4. Velocity of a steel bead of diameter 1 mm (solid line), compared to simulation without memory force (dashed) and with Stokes memory (dash-dotted). The inset shows an enlargement near the onset of motion. The Reynolds number, based on the limit velocity is 430. The sphere velocity profile results from averaging $n = 10$ successive experiments.

2.4 Simulation

In order to draw some comparison between our measurements and the models mentioned in Section 1, we compute numerical solutions of equation (4), in the case of a fluid at rest:

$$(m_{\rm p} + \frac{1}{2}m_{\rm f})\frac{{\rm d}\mathbf{v}_{\rm p}}{{\rm d}t} = (m_{\rm p} - m_{\rm f})\mathbf{g} - \frac{1}{2}\pi a^2 \rho_{\rm f} \|\mathbf{v}_{\rm p}\| \mathbf{v}_{\rm p} c_{\rm D}(Re) + \mathbf{F}_{\rm history}. \quad (7)$$

We have considered either the case of no memory, or the diffusive kernel of equation (1), named respectively "no memory" and "Stokes memory" simulation for convenience. The numerical scheme uses a fourth order Runge-Kutta in time and Newton-Cotes formulas for the history terms.

3 Results

3.1 General features

We first discuss features that are common to all measurements. As an example, we present in Figure 4 the velocity measurement for a steel bead with diameter 1 mm. Starting from rest, the bead has a monotonous acceleration and reaches a terminal velocity. From this measurement, we compute the drag coefficient and compare it to standard measurements made on fixed spheres (Sect. 3.2).

We also show in Figure 4 velocity profiles computed from equations of motion without memory term and with a Stokes memory force. The actual motion shows that while there has to be a memory force as in equation (7), it does not follow the Stokes expression at all times (as explained above, the deviation at very small time – $t < 5$ ms – is an artifact of the algorithm). This is discussed in Section 3.3.

We observe that two control parameters influence the dynamics of the fall: the Reynolds number (see Sect. 3.4) and the density of the particle (discussed in Sect. 3.5). In all cases we note that the asymptotic state of motion is stationary and that the limit velocity is reached in a finite time.

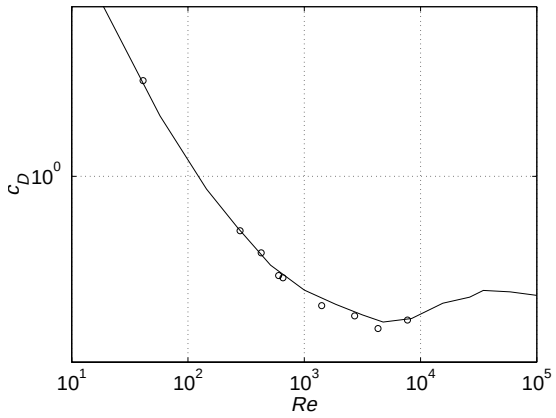

Fig. 5. Empirical curve (solid) for the drag coefficient (from reference [12]) *versus* Reynolds number and our experimental measurements (o).

3.2 Drag

We measure the limit velocity $V_{\rm l}$ for every configuration given in Table 1. In each case the motion has reached a stationary state, so that $V_{\rm l}$ is well defined. All measurements are made on velocity profiles obtained after averaging about 10 realisations – transient effects are discussed in Section 3.5. Knowing the limit velocity $V_{\rm l}$ of a bead, we calculate the drag coefficient by removing non stationary terms in equation (7) and obtain $c_{\rm D}(Re)$:

$$c_{\rm D} = \frac{8ag(d-1)}{3V_{\rm l}^2}\,. \quad (8)$$

In the calculation of the Reynolds number we use the value for the viscosity of water at 25 °C, $\nu = 0.89 \times 10^{-6}$ m^2 s^{-1} [11] – a value confirmed by an independent measurement with a Ubbelhode viscosimeter. Our experimental curve $c_{\rm D}(Re)$ is given in Figure 5, where it is compared to standard empirical drag measurements [12]. The results are in good agreement: the drag coefficient is the same in the case of a fixed sphere and in the case of a free settling bead. It is generally admitted this should be true at low Reynolds number, where numerical and analytical studies agree that the drag is indeed given by the Stokes expression. However, at higher Reynolds numbers this result is not so obvious. Indeed, it may be surprising that the particle reaches a stationary limit velocity, and thus probably a stationary momentum flux across the wake (see also Sect. 3.5). This is an important difference with observations of the wake past a *fixed* sphere [13,14] where

the incoming flow is set at a constant uniform speed and the force acting on the body may there take any value. In that case, instabilities in the wake are known to exist and are related to vortex shedding. In our case, the constraint is just that the forcing gravity is constant, any change on the force felt by the sphere must be related to a change on the fluid motion. One also notes that for fixed bodies near the onset of vortex shedding, only averages of the drag force are reported and the matter may deserve further investigations, see [15].

We emphasize that in a given experiment the limit velocity is *a priori* unknown, it results from the balance of gravity and drag forces, which are in turn Reynolds number dependent. From equation (7), one obtains an implicit equation for the Reynolds number:

$$Re^2 c_{\mathrm{D}}(Re) = \frac{32a^3(d-1)g}{3\nu^2}\,. \qquad (9)$$

In any experiment one chooses the density of the sphere and its size; the Reynolds number is set by the dynamics of the motion.

3.3 Memory effect

We now address the question of the cumulative effect of the development of the wake on the body motion, *i.e.* the "memory effect". To wit, we use experiment #5 as an example (steel bead with diameter $2a = 1$ mm). We compare the measured velocity profile to numerical resolution of equation (7) first without memory term and then with Stokes memory – see Figure 4. For short times ($t < 30$ ms), one observes a deviation from the behaviour that would be in the absence of memory. The recorded velocity of the sphere is close to the simulation with Stokes memory, for times less than 20 ms. At times larger than 20 ms, the measured velocity separates from the Stokes memory curve (almost by necessity since the Stokes approximation is valid only in the near wake). The bead then reaches its limit value for $t \sim 300$ ms. An interesting feature is that the measured velocity profile always lies between the two simulated curves: Stokes term, which corresponds to 'infinite memory' and no memory at all.

To investigate further, we have derived from our measurement the memory force term, computed as the total force (obtained from the velocity derivative) minus the gravity and drag terms. Figure 6 compares the result with the Stokes memory simulation. Despite the noise of the measurement, one observes that the two curves have similar shapes. In particular the memory force reaches a maximum for a time that is correctly given by Stokes' approximation, although the actual memory force is always smaller. The differences are more marked at later dates. The Stokes memory term loses only 50 percent of its peak value in 0.25 s whereas the measured memory term vanishes in the same time (within experimental precision). These results are in agreement with numerical simulations of Lawrence and Mei [8]: for small times we observe a Stokes behaviour and for longer times the decrease of the transient term is much more rapid than $t^{-\frac{1}{2}}$. The authors predict, in the limit of very long times, a t^{-2} behaviour, after a strong, possibly exponential, decrease of several orders of magnitude of the transient force in the case of an abrupt change of velocity. If a similar phenomenon occurs in our case, after an abrupt decrease, the asymptotic term may be smaller than the finite accuracy of our measurement (which comes from the finite size of the pixels in time-frequency pictures, from acoustical and electromagnetic noises).

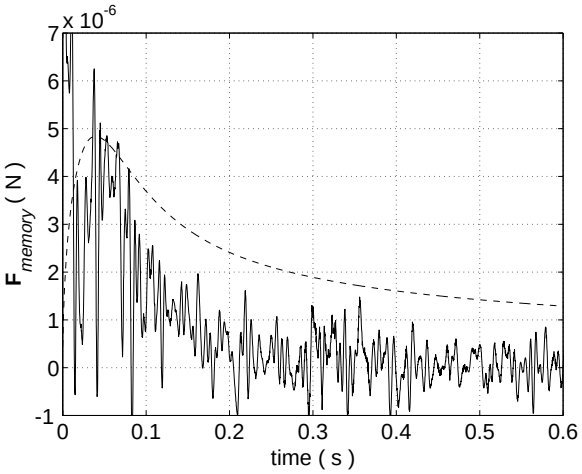

Fig. 6. The memory term of equation (7) calculated from the measured velocity of the sphere of the previous figure.

We note that in all the experiments the sphere experiences a Stokes-like history force during the early stage of motion, until a significant fraction of the terminal velocity is reached (between 1/3 and 1/2 of V_{l}). This may correspond to quite high instantaneous Reynolds numbers ($Re \sim 300$ in experiment #5). The memory term has thus a significant contribution despite the fact that the amplitude of the history force is at best a tenth of the particle weight.

3.4 Reynolds number effects

Velocity variations at various Re are given in Figures 7 and 8 for experiments #1,4,6,7,8.

We first discuss curve #1, which corresponds to a glass bead of diameter equal to 0.5 mm. It has the lowest Reynolds number, about 40, achieved in our experiments and falls into the range of Re values where numerical simulations have been reported by Lawrence and Mei [8]. We observe that its behaviour is quite similar to that of all of our measurements: a Stokes memory behaviour at short times and a transition period where the bead reaches its limit velocity in a finite time – long, power law memory behaviour is not detected.

In order to investigate the Reynolds number dependence and to separate it from density effects, we use steel spheres with varying diameter – see Figure 8. We see that the evolution is qualitatively similar for all the beads: the sphere reaches its limit velocity in a finite time. The value

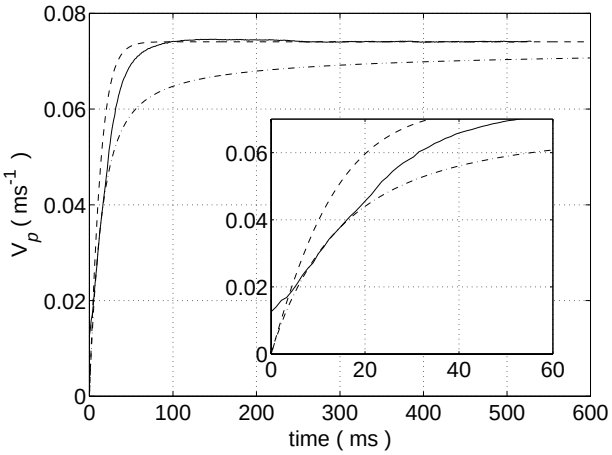

Fig. 7. Velocity profiles in experiments #1. The Reynolds number, based on the limit velocity is equal to 41.

of this limit and the time it takes to reach it depend on the size of the bead. We define a characteristic time τ_{95} as the time it takes for the bead to reach 95% of the limit speed – numerical values are given Table 1. A general dimensional analysis of the problem gives the following expression for τ_{95}:

$$\tau_{95} = \left(\frac{a}{g}\right)^{\frac{1}{2}} F(Re, d), \tag{10}$$

where F is *a priori* some function of density and Reynolds number. If one subsequently uses equation (7) without the history term, one obtains a characteristic time:

$$\tau_0 = \sqrt{\frac{8}{3}}\sqrt{\frac{a}{c_{\mathrm{D}0}g}}\frac{d+\frac{1}{2}}{\sqrt{d-1}}, \tag{11}$$

where $c_{\mathrm{D}0}$ is the drag coefficient based on the terminal velocity and contains the Reynolds number dependency. However, we observe that our measurements show almost no Reynolds number dependence when τ_{95} is non-dimensionalized by $(a/g)^{\frac{1}{2}}$, see Figure 9: the characteristic time for our Reynolds interval is almost $(a/g)^{\frac{1}{2}}$ (for a given particle density) which is a convective time. For very low Reynolds numbers, neglecting the history integral, one would predict a diffusive time a^2/ν. These points confirms that for Reynolds numbers much greater than 1 the nature of the phenomena involved in the bead motion changes from diffusion to advection. We also note that the memory terms must be taken into account at Reynolds numbers up to 4000 in order to correctly describe the particle acceleration.

Assuming now that the drag coefficient is known from reference tables, and given the above discussion on the characteristic time, we re-plot the velocity variations non dimensionalized by V_{l} and as a function of $t^* = t/(a/g)^{\frac{1}{2}}$ (see Fig. 10). In that manner, after Stokes regime, all the curves surprisingly collapse onto a single exponential shape:

$$\frac{v_{\mathrm{p}}}{V_{\mathrm{l}}} = 1 - \exp\left(-\frac{3t}{\tau_{95}}\right). \tag{12}$$

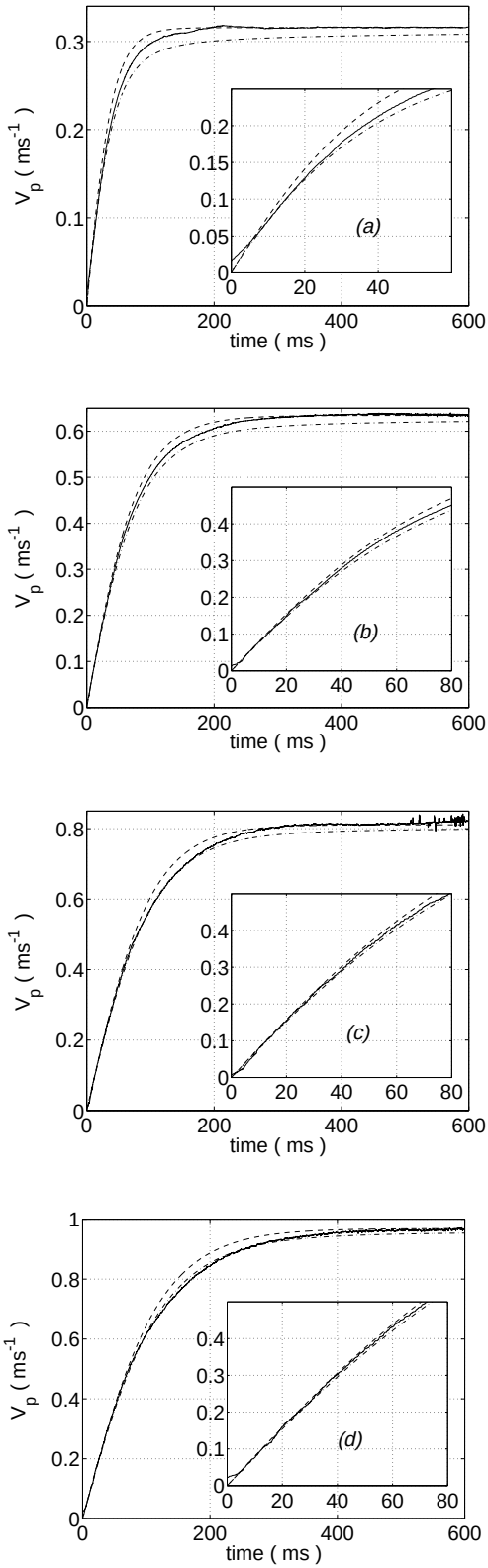

Fig. 8. Velocity profiles in experiments #4 (a), 6 (b), 7 (c), 8 (d) corresponding to steel beads with diameter 0.8, 2, 3, 4 mm – see Table 1.

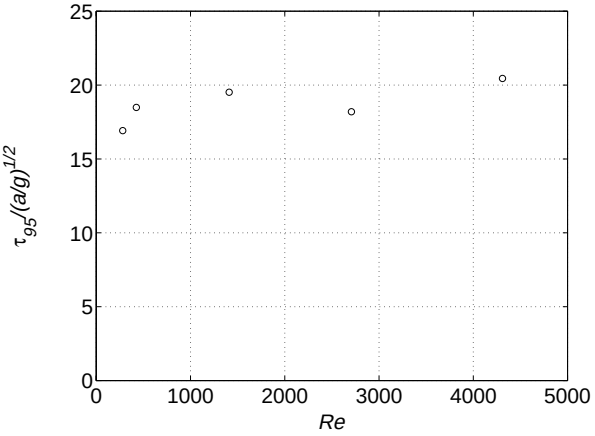

Fig. 9. Characteristic time τ_{95} nondimensionnalized by $(a/g)^{\frac{1}{2}}$ *versus* Reynolds numbers for the steel spheres of diameters from 0.8 to 4 mm.

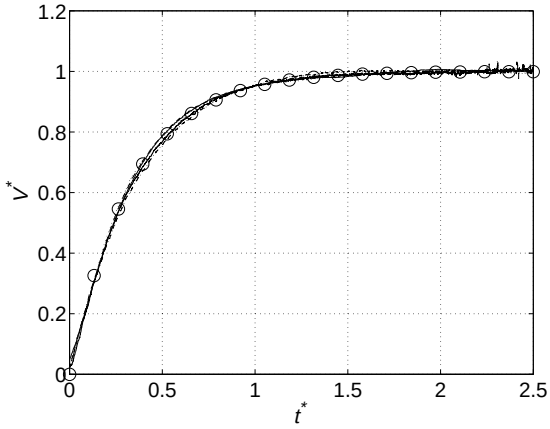

Fig. 10. Velocity measurements in non-dimensional units for the steel spheres of diameters from 0.8 to 4 mm. The ∘ symbols represent the exponential of equation (11).

This observation may be of value for the intermediate time modeling of a particle in varying flow conditions, as may occur in turbulence.

Lastly, inspection of the largest Reynolds number available shows an interesting phenomenon, as in Figure 11 where we present the result for the 6 mm steel bead – experiment #9. At moderate Reynolds number we have noted that the velocity profile lies in between the Stokes and no-memory curves. This is not so here; the bead first accelerates with no memory force ($t < 80$ ms) and then experience an abrupt reduction of its acceleration (from $a_1 = 6\ \mathrm{m\,s^{-2}}$ to $a_1 = 3.6\ \mathrm{m\,s^{-2}}$ in less than 20 ms). In this process, its velocity becomes lower than its Stokes value. However, the velocity still reaches its limit value in a finite time of the order of $(a/g)^{\frac{1}{2}}$, a rather subtle compensation of a start with little memory effect followed by a regime with 'more than Stokes' memory. The limit value is in agreement with the empirical drag coefficient. We stress that this behaviour is quite reproducible and that precursors of it, although shallow, can be detected on our recordings for the 3 and 4 mm spheres. Such an

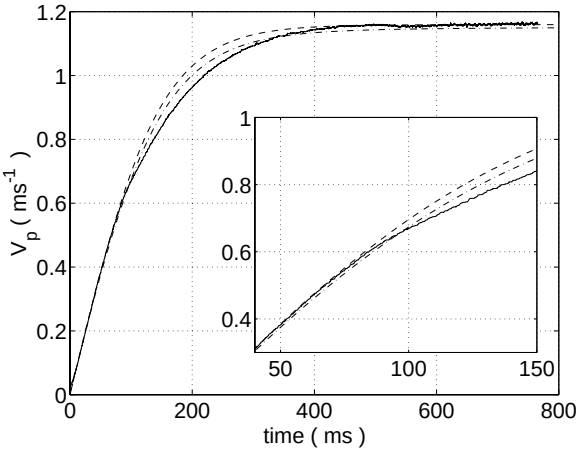

Fig. 11. Velocity measurement and corresponding simulations for the 6 mm steel sphere $Re = 7700$.

abrupt change must be related to a change in the particle wake; it appears for Reynolds numbers greater than 3 000 and seems to increase with the diameter of the bead.

3.5 Density effects

The density $d = \rho_\mathrm{p}/\rho_\mathrm{f}$ appears in equation (7) in two ways. First in the gravity term the quantity $d - 1$ takes into account buoyancy and enters in the effective gravitational mass. Density appears in a different way in the effective inertial mass: in that case it is $d + \frac{1}{2}$. Indeed from equation (7) one has:

$$\frac{\mathrm{d}v_\mathrm{p}}{\mathrm{d}t} = \frac{3}{8}\frac{v_\mathrm{p}^2 c_D(Re)}{a(d+\frac{1}{2})} - \frac{d-1}{d+\frac{1}{2}}g + \frac{F_\mathrm{history}}{m_\mathrm{f}(d+\frac{1}{2})}\cdot \qquad (13)$$

The effective drag and gravity vary as $(d-1)/(d+1/2)$ whereas the memory term varies as $1/(d+1/2)$. Its contribution is enhanced at lower density.

Thus by changing the value of density we vary the ratio of inertial to gravitational mass and we expect to observe different dynamical behaviours. In particular, we expect the motion of a lighter bead to be more influenced by the eventual unsteadiness of its wake. In Figure 12a,b we compare two beads with Reynolds numbers close to 400 (glass and steel) or 630 (tungsten carbide and glass) without any averaging. In both cases, we can see that the velocity of the glass bead presents oscillations while approaching its limit value. Such oscillations must be linked to a temporal evolution of the particle wake. One observes that the velocity is no longer a monotonous function of time: it alternates periods of increase and decrease. For this to happen, the acceleration of the particle must change sign; in particular the reaction of the wake on the particle is sufficient to overcome the (reduced) gravitational force. It is not observed for the denser metal spheres.

The oscillations disappear if the motion is averaged over several falls – see Figure 12c,d. In that way, we obtain roughly equal τ_{95} characteristic times for the beads

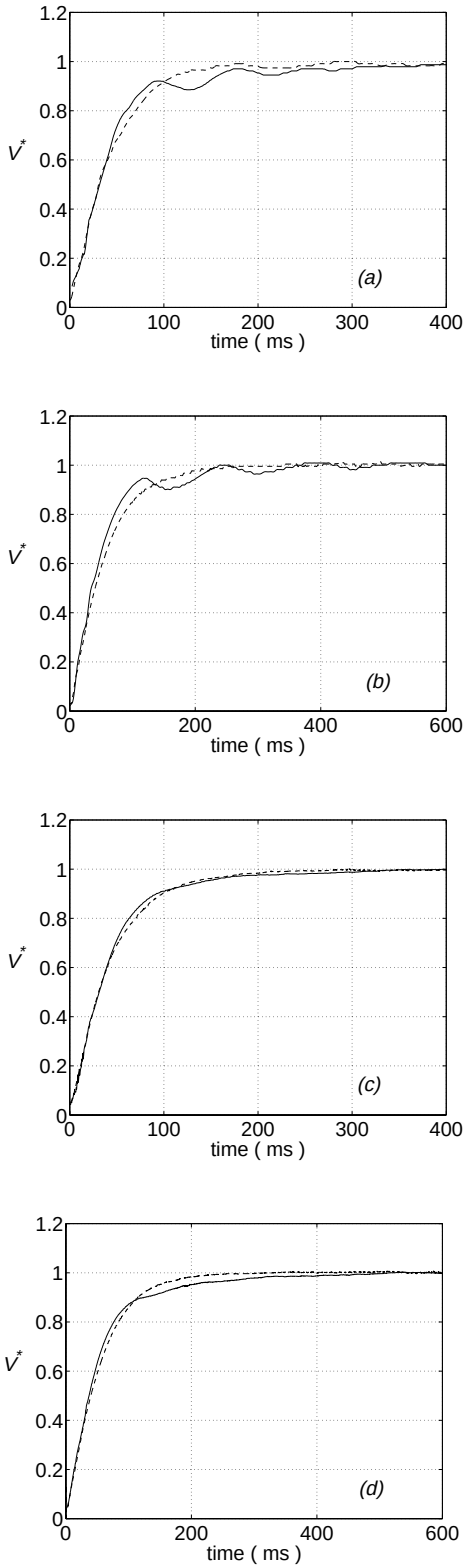

Fig. 12. Velocity measurement without averaging for (a) tungsten carbide D = 1 mm (dashed) and glass D = 2 mm (solid) $Re \sim 400$ and (b) steel D = 1 mm (dashed) compared with glass D = 1.5 mm (solid) $Re \sim 630$. (c) and (d) are equivalent plots for the motion averaged over 10 experiments.

of all densities. The vanishing of the oscillations when averaging shows that the events in the wake that are responsible for them are not coherent, in the sense that they do not occur at fixed times (phases). It is tempting to associate these events with the vortex shedding that may occur at these Reynolds numbers (for a fixed sphere the threshold is $Re_c \sim 250$). However we note that the oscillations are slower than what is reported for a fixed sphere: we measure an effective Strouhal number $St \sim 0.05$ (see Fig. 12b) whereas Sakamoto and Haniu [14] indicates $St \sim 0.2$ for $Re \sim 500$. Finally, we observe that the oscillations are damped. Within the limits of our resolution and experimental apparatus it is not possible to state on the persistence of (small) oscillations in the limit of very large times.

4 Concluding remarks

We have implemented a continuous tracking of the Doppler shift of the ultrasound backscattered by a moving particle. This method is an extension with a high resolution in time of the classical pulsed radar and sonar techniques.

We have considered the existence of memory effects that result from the hydrodynamical interaction between a moving sphere and its wake in the case of a settling bead in a fluid at rest. In the case of particles much denser than the fluid, and at intermediate Reynolds number, our results are in qualitative agreement with numerical simulations of [4,8,9]: we observe a memory term varying as $t^{-1/2}$ at short times, followed by an exponential decrease. We note that memory effects have a significant influence at Reynolds numbers of a few thousand. The motion of the bead can be interpreted as resulting from the interaction with the wake. At small Reynolds number it has a Stokes-like behavior due to the simple diffusion of vorticity; at later stages one must also take into account advection effects and the 'memory' term becomes gradually more complex. In particular, the eventual non stationarity of the wake may lead to very complex transient dynamics.

The case of lighter beads shows that density is another control parameter. For Reynolds numbers of a few hundreds, we observe a behaviour not yet described by analytical nor numerical work: the velocity of the particle shows transitory oscillations while reaching a stationary limit value. We propose that this may be due to transient vortex shedding in the wake of the sphere which reacts on the motion of the particle. This is an important difference with the case of a sphere constrained to move at a constant speed (or equivalently fixed in a flow at constant speed); in that case the force felt by the sphere oscillates continuously at the frequency of vortex shedding. In our case here, the bead is forced with a constant gravity and we observe that its limit speed is stationnary. This matter certainly deserves further investigations.

We thank Vermon for conception and maintenance of the ultrasonic transducers, O. Michel and P. Flandrin for helpful discussions on the reassignment technique.

References

1. M.R. Maxey, J.J. Riley, Phys. Fluids **26**, 883 (1983).
2. T.R. Auton, J.C.R. Hunt, M. Prud'homme, J. Fluid Mech. **197**, 241 (1988).
3. M. Rivero, J. Magnaudet, J. Fabre, C. R. Acad. Sci. Paris II **312**, 1499 (1991).
4. E.J. Chang, M.R. Maxey. J. Fluid Mech. **303**, 133 (1995).
5. P.M. Lovalenti, J.F. Brady, J. Fluid Mech. **256**, 561 (1993).
6. H. Schlichting, *Boundary layer theory*, 7th edn. (Mc Graw-Hill, 1979).
7. G. Sridhar, J. Katz. Phys. Fluids, **7**, 389 (1995).
8. C.J. Lawrence, R. Mei. J. Fluid Mech. **283**, 307 (1995).
9. I. Kim, S. Elghobashi, W.A. Siriginano, J. Fluid Mech. **367**, 221 (1998).
10. F. Auger, P. Flandrin, IEEE Trans. Sig. Proc. **43**, 1068 (1995).
11. R.C. Weast. *Handbook of chemistry and Physics*, 60th edn. (CRC Press, 1981).
12. F.W. Roos, W.W. Willmarth, AIAA Journal **9**, 285 (1971).
13. R. Natarajan, A. Acrivos, J. Fluid Mech. **254**, 323 (1993).
14. H. Sakamoto, H. Haniu, J. Fluid Mech. **287**, 151 (1995).
15. R. Hernandez-Pellicer, Ph.D thesis, École Normale Supérieure de Lyon, 1999.